Deciphering the evolution of supramolecular nanofibers in solution and solid-state: a combined microscopic and spectroscopic approach

Subhankar Kundu, Arkaprava Chowdhury, Somen Nandi, Kankan Bhattacharyya,* and Abhijit Patra*

Department of Chemistry, Indian Institute of Science Education and Research Bhopal, Bhopal Bypass Road, Bhauri, Bhopal 462066, Madhya Pradesh, India

Email: abhijit@iiserb.ac.in, kankan@iiserb.ac.in

Contents

I. Materials and methods

1.1. Chemicals: All chemicals were used as received unless otherwise mentioned. 2,5-Thiophenediylbisboronic acid (≥95.0%), 4-bromobenzaldehyde (99%), potassium carbonate (≥99.0%), tetrakis(triphenylphosphine)palladium(0) (99%), 2-pyridylacetonitrile (99%), benzyl cyanide (99%), piperidine (≥99.5%), chloroform-d (99.8 atom% D), dimethyl sulfoxide-d_6 (99.9 atom% D), Nile Red (≥98%) were received from Sigma-Aldrich. Lysotracker deep red, mitotracker red, cellmask deep red, Dulbecco's modified eagle medium (DMEM), phosphate-buffered saline (PBS), and fetal bovine serum (FBS) were received from Thermofisher Scientific. All spectroscopic grade solvents (n-hexane, toluene, chloroform, tetrahydrofuran, and dimethyl sulfoxide) were obtained from Spectrochem. Anhydrous sodium sulfate was received from SD Fine-Chem Limited. Celite was received from Spectrochem. Dichloromethane, n-hexane, and ethyl acetate were distilled prior to use.

1.2. Instrumentation:

Nuclear magnetic resonance (NMR) spectroscopy: ^{1}H NMR and ^{13}C NMR spectra were recorded using Bruker Avance III NMR spectrometers. The residual solvent signal was used as an internal standard, and chemical shifts (δ) were reported in parts per million (ppm). All NMR measurements were carried out in $CDCl_3$ at room temperature.

High-resolution mass spectrometry (HRMS): High-resolution mass spectrometry (HRMS) data were obtained using Bruker MicrOTOF-Q-II mass spectrometer instrument.

Melting point measurements: Melting points of the compounds were measured using Digital Melting Point Apparatus (Jyoti: AN ISO: 9001:2000, India). Compounds were loaded in the capillary glass tubes.

Field Emission scanning electron microscopy (FESEM): The morphologies of the TPAn dispersions were observed using Carl Zeiss (Ultraplus) field emission scanning electron microscope. Samples for microscopy were prepared by drop-casting of TPAn dispersion (~ 10 µL) on Si wafer. After drying under a vacuum, all samples were coated with a thin layer of sputtered gold before imaging. The accelerating voltage of 20 kV was used for imaging.

Transmission electron microscopy (TEM): The TEM analysis was carried out using the FEI TALOS 200S instrument at a working voltage of 200 kV. The samples for TEM analysis were prepared by drop-casting the dispersions of TPAn and TPAnWN over a carbon-coated 400 mesh Cu grid.

Atomic force microscopy (AFM): The atomic force microscopy (AFM) images were obtained using Agilent 5500 AFM/SPM in tapping mode (silicon noncontact probe; tip radius ~ 8 nm; force constant = 0.5 N m^{-1}).

Steady-state absorption spectroscopy: Cary 100 spectrophotometer was used for the measurements of the UV-Visible absorption spectra. 10 mm path length quartz cuvettes were used for recording the spectra. The optical density was kept low (< 0.1) to avoid artifacts due to inner filter effects. The solid-state absorption spectra were recorded using the same spectrometer equipped with a diffuse reflectance integrating sphere attachment (DRA).

Steady-state fluorescence spectroscopy: Jobin Yvon Horiba Model Fluorolog-3-21 instrument was used for all the steady-state fluorescence measurements.

Time-resolved fluorescence spectroscopy: Time-correlated single-photon counting (TCSPC) spectrometer (Delta Flex-01-DD/HORIBA) was used to carry out the time-resolved fluorescence measurements. 373 and 407 nm delta diode lasers were used as the excitation sources.

Fluorescence Quantum Yield (ϕ_f) Measurements: The fluorescence quantum yield of TPAn in solution was estimated using coumarin 153 dye in ethanol (Φ_f = 38%) as the reference dye using the following equation.[1]

$$\Phi_{f,x} = \Phi_{f,s} \times \frac{F_x}{F_s} \times \frac{f_s}{f_x} \times \frac{n_x^2}{n_s^2} \text{ ……...(S1)}$$

Where Φ_f is the fluorescence quantum yield, subscript x denotes sample, and subscript s refers to the standard. F denotes integral fluorescence; n refers to the refractive index of the solvent used in the measurements, and f is the absorption factor at the excitation wavelength given by the following equation.

$$f = 1 - 10^{-A(\lambda_{ex})} \text{ ……..(S2)}$$

Where A is absorbance and ε = molar extinction coefficient in L mol^{-1} cm^{-1}.

The absolute quantum yields for solid samples were measured using a calibrated integrating sphere (Quanta-Phi, Horiba).

Preparation of TPAn aggregates: A stock solution of 0.2 mM was prepared by adding 1 mg of TPAn in 10 mL of THF. 30 μL of the stock solution was rapidly added to the binary solvent mixture of THF-water under sonication for 1 min. A similar procedure was followed to prepare the aggregates in a DMSO-water mixture. The pH of the dispersion medium was monitored using a calibrated pH meter (Oakton). The pH meter was calibrated using standard buffer solutions of pH = 12, 7, and 4.

Confocal Microscopy: PicoQuant, MicroTime 200 confocal set up (inverted optical microscope; Olympus IX-71) was used for the fluorescence correlation spectroscopy (FCS) analysis.[2] The time-tagged time-resolved (TTTR) mode was used to collect the data. IGOR-Pro software (WaveMetrics, USA) was used to fit the correlation curves. Electron-multiplying charge-coupled device (Newton EMCCD, ANDOR Technology) attached to a spectrograph

(Keymera, ANDOR Technology) was used to record the luminescence spectra inside the HeLa cells.

Computational Investigations: The ground-state geometry optimized structure of TPAn was computed using the Gaussian 09 program package. The density functional theory (DFT) calculation was carried out at the B3LYP/6-31G(d,p) level.

Powder X-ray diffraction (PXRD) analysis: The XRD measurement was performed using a PANalytical Empyrean X-ray diffractometer in the Bragg-Brentano geometry using a Cu-$K_{\alpha 1}$ (λ = 1.5405 Å) radiation and Ni beta filter was used to obtain only the K_{α} radiation. The powder samples were mounted on the silicon zero background holder by dropping powder and then flatten the sample surface with a glass plate. The generator power sets at 45 kV and 40 mA to measure the powder X-ray data. The data were collected using the Pixcel^{3D} detector in the angular range of 2 to 80° in the 2θ range within steps of 0.013°.

Cell Culture: The growth media for the HeLa cells was prepared through mixing the phenol red-free DMEM (Dulbecco's modified eagle medium), 10% fetal bovine serum (FBS), and 1% pen strep glutamine (from Gibco). 5% (v/v) CO_2 enriched air at 37 °C was implemented for the cell growth. Tissue culture confocal Petri dish (Tarsons) was used for the seeding of the cells. The cells were seeded for 24 h before the treatment of TPAn and Nile red. It was noticed that the presence of FBS reduced the fluorescence intensity of TPAn. FBS contains several components like bilirubin, cholesterol, creatinine, urea, Na^+, Cl^-, K^+, Ca^{2+}, Mg^{2+}, glucose, albumin, etc. The interaction between TPAn and the components of FBS could reduce the fluorescence intensity. Hence, FBS free DMEM was used to prepare 2 mL of 30 nM TPAn solution. Then, the solution was added to the confocal dish and the incubation was done for 15 min. Subsequently, the cells were washed thoroughly for three times by phosphate-buffered saline (PBS) to ensure the elimination of free dye outside of the cell surface. Then, 2 mL serum-free media (FluoroBrite DMEM) was added to the confocal dish for the imaging.

II. Synthesis and characterizations

2.1. Synthesis of 4,4'-(thiophene-2,5-diyl)dibenzaldehyde (TBA):

TBA was synthesized following a reported procedure with minor modifications (Scheme S1).[3] 2,5-Thiophenediylbisboronic acid (2.91 mmol) and 4-bromobenzaldehyde (5.82 mmol) were taken in a Schlenk tube. Then potassium carbonate (2 mmol) was added into the reaction tube. The Schlenk tube was wrapped with aluminium foil to protect from light. Tetrakis(triphenylphosphine)palladium(0) was added into the Schlenk tube under the inert atmosphere of Argon. 15 mL of dry THF and 5 mL of degassed water were added to the reaction mixture and heated at 80 °C for 24 h under continuous stirring. After cooling and dichloromethane (DCM) addition, the reaction mixture was washed with water and dried on sodium sulfate. It was then run through a celite column to remove the Pd-species. The obtained solution was then dried under reduced pressure. The dark yellow crude residue was purified through silica gel column chromatography using 10% EtOAc-hexane as eluent to obtain a yellow product (yield 55%). The structure of TBA was obtained from crystal structure analysis, which was corroborated with the reported one (CCDC: 1564775).[4]

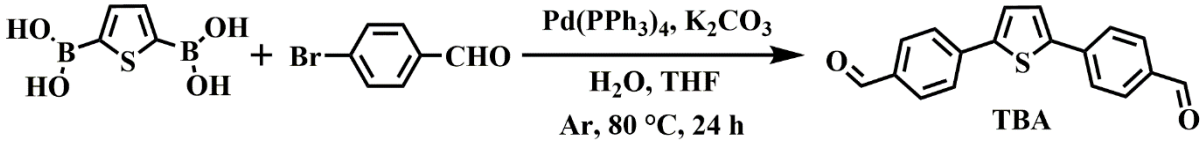

Scheme S1 Synthetic scheme for TBA through Suzuki coupling reaction.

^{1}H NMR (500 MHz, $CDCl_3$ δ_H): 10.02 (s, 2H), 7.92 (d, *J* = 8.2 Hz, 4H), 7.80 (d, *J* = 8.2 Hz, 4H), 7.49 (s, 2H).

^{13}C NMR (126 MHz, $CDCl_3$ δ_C): 191.35, 143.87, 139.47, 135.46, 130.56, 126.32, 125.94.

HRMS: Calculated for $C_{18}H_{12}O_2S$: 293.0631 g mol^{-1}; found: 293.0658 g mol^{-1} [M+H$^+$].

Melting point: 240 °C.

2.2. Synthesis of 3,3'-(thiophene-2,5-diylbis(4,1-phenylene))bis(2-(pyridin-2-yl)acrylonitrile) (TPAn):

TBA (0.34 mmol) and 2-pyridylacetonitrile (0.68 mmol) were mixed in ethanol and stirred inside a Schlenk tube. A catalytic amount of piperidine (1.36 mmol) was added into the reaction tube. The reaction mixture was refluxed at 85 °C for 12 h under continuous stirring. Then, the obtained orange precipitate was washed several times with ethanol and hexane through centrifugation. An orange-colored solid was obtained with a 48% yield (Scheme S2).

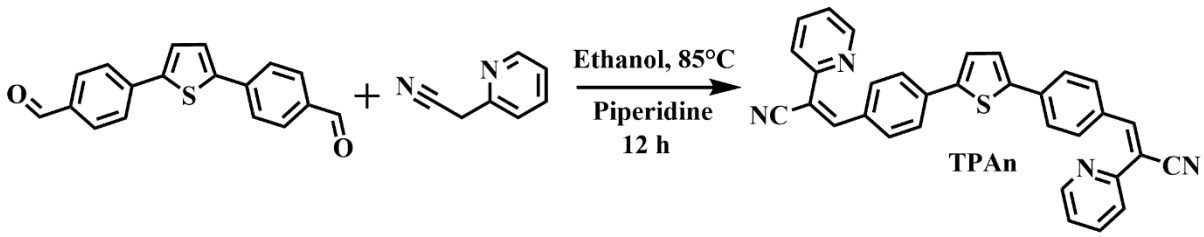

Scheme S2 Synthetic scheme for TPAn through Knoevenagel condensation reaction.

^{1}H NMR (500 MHz, $CDCl_3$ δ_H): 8.66 (d, 2H), 8.49 (s, 2H), 8.06 (d, 4H), 7.83-7.74 (m, 8H), 7.46 (s, 2H), 7.30 (m, 2H).

^{13}C NMR (126 MHz, $CDCl_3$ δ_C): 151.28, 149.82, 144.31, 143.86, 137.58, 136.66, 132.77, 130.92, 126.02, 125.75, 123.65, 121.49, 118.13, 109.76.

HRMS: Calculated for $C_{32}H_{20}N_4S$: 493.1481 g mol^{-1}; found: 493.1496 g mol^{-1} [M+H$^+$].

Melting point: 260 °C (decomp.).

2.3. Synthesis of 3,3'-(thiophene-2,5-diylbis(4,1-phenylene))bis(2-phenylacrylonitrile) (TPAnWN):

TBA (0.34 mmol) and benzyl cyanide (0.68 mmol) were mixed in ethanol and stirred inside a Schlenk tube. A catalytic amount of piperidine (1.36 mmol) was added into the Schlenk tube. The reaction mixture was refluxed at 85 °C for 12 h under continuous stirring. Then, the obtained yellow precipitate was washed several times with ethanol and hexane through centrifugation. A yellow-colored solid was obtained with a 63% yield (Scheme S3).

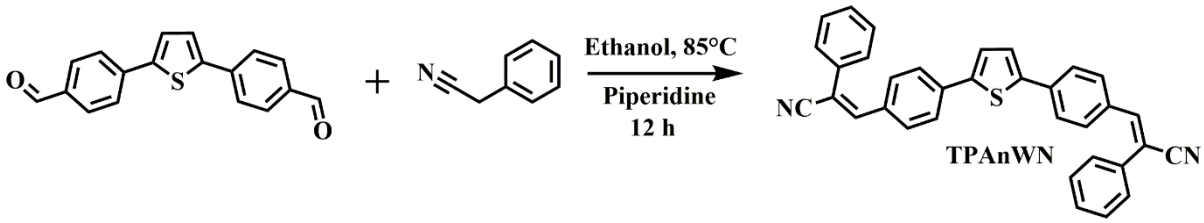

Scheme S3 Synthetic scheme for TPAnWN through Knoevenagel condensation reaction.

^{1}H NMR (400 MHz, $CDCl_3$ δ_H): 7.96 (d, 4H), 7.80-7.65 (m, 8H), 7.54 (s, 2H), 7.51-7.38 (m, 8H).

^{13}C NMR: We were unable to record the ^{13}C NMR for TPAnWN due to the low solubility in all common organic solvents.

HRMS: Calculated for $C_{34}H_{22}N_2S$: 491.1576 g mol^{-1}; found: 491.1588 g mol^{-1} [M+H$^+$].

Melting point: 260 °C (decomp.).

III. Computational study

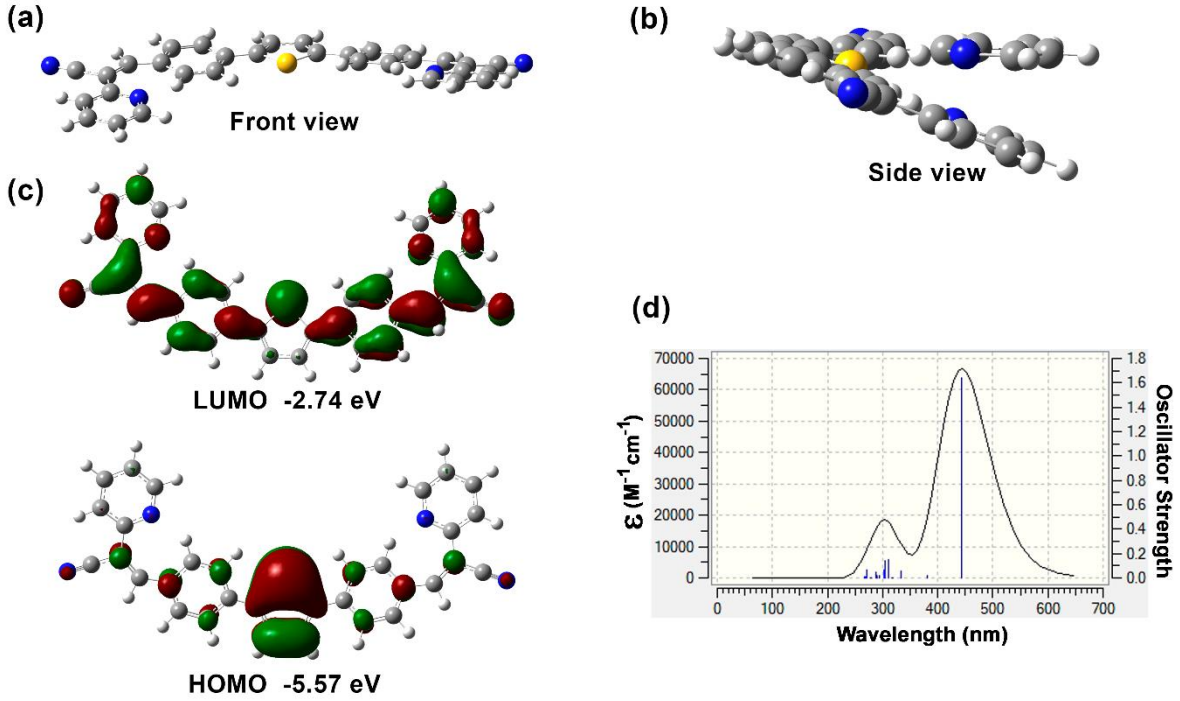

Fig. S1 (a, b) Geometry optimized structures, and (c) the distributions of electron density in the highest occupied molecular orbital (HOMO), the lowest unoccupied molecular orbital (LUMO), and the respective energy values (eV) of TPAn obtained using density functional theory (DFT) calculations at B3LYP/6-31G(d,p) level. (d) Theoretical UV-Vis absorption spectrum of TPAn obtained using the time-dependent density functional theory (TDDFT) at B3LYP/6-31G(d,p) level.

The ground-state optimized structure of TPAn was obtained by density functional theory (DFT) calculations at the B3LYP/6-31G (d,p) level. Fig. S1a and S1b indicate that both the pyridoacetonitrile units are not in the same plane with respect to the plane belonging to the central thiophene unit. Thus, molecular geometry inhibits the π-π stacking interactions leading to the solid-state emission. However, the extended conjugation from the donor thiophene unit to the acceptor -CN moiety (linear) led to the red-shifted emission as compared to that of 4,4'-(thiophene-2,5-diyl)dibenzaldehyde (TBA). The distributions of electron density in the highest occupied molecular orbital (HOMO) and the lowest unoccupied molecular orbital (LUMO) of TPAn are shown in Fig. S1c. The HOMO is located mostly on the thiophene unit. Whereas, the LUMO is distributed on the overall molecule. The time-dependent density functional theory (TDDFT) calculations at the B3LYP/6-31G (d,p) level was employed to obtain the theoretical UV-Vis absorption spectrum of TPAn, which was corroborated well with the experimental results (Fig. S1d).

IV. Spectroscopic investigation

4.1. Steady-state absorption, emission, and lifetime measurements in solution:

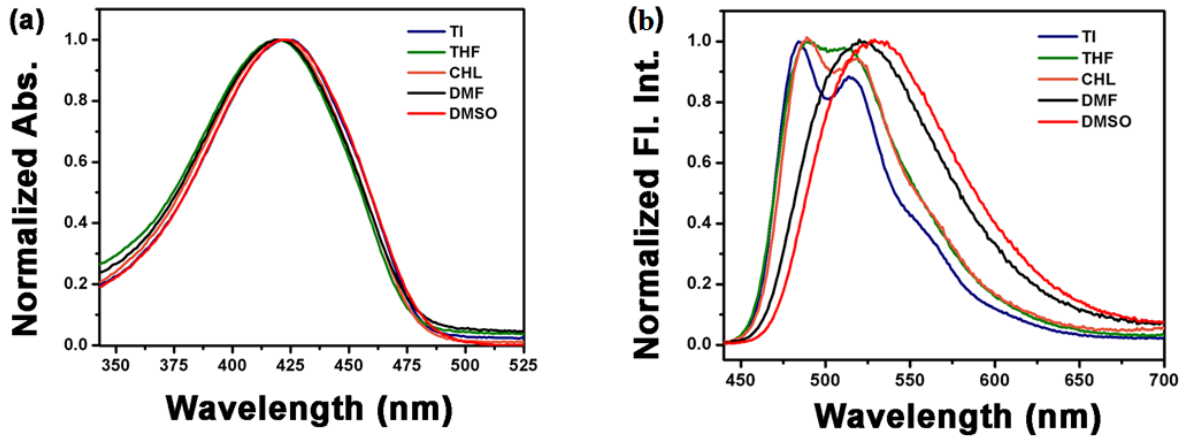

Fig. S2 Normalized (a) absorption and (b) emission spectra (excited at individual λ_{abs}^{max}) of TPAn (5 μM) in the solvents (Tl = toluene, THF = tetrahydrofuran, CHL = chloroform, DMF = *N*, *N*-dimethylformamide, DMSO = dimethyl sulfoxide) of varying polarity.

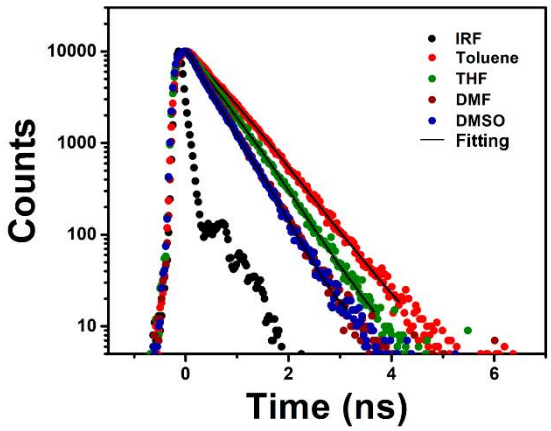

Fig. S3 Emission decay profiles of TPAn (λ_{ex} = 407 nm, λ_{em} = 525 nm) in different solvents with varying polarity.

Fig. S2 represents the normalized absorption and emission spectra of TPAn in different solvents of varying polarity. TPAn showed a mono-exponential decay profile in all solvents (Fig. S3). The lifetime of TPAn showed a steady decrease with an increase in the polarity of the solvent medium. Fig. S4 demonstrates the excitation-independent emission property of TPAn. The spectroscopic features of TPAn in different solvents are summarized in Table S1.

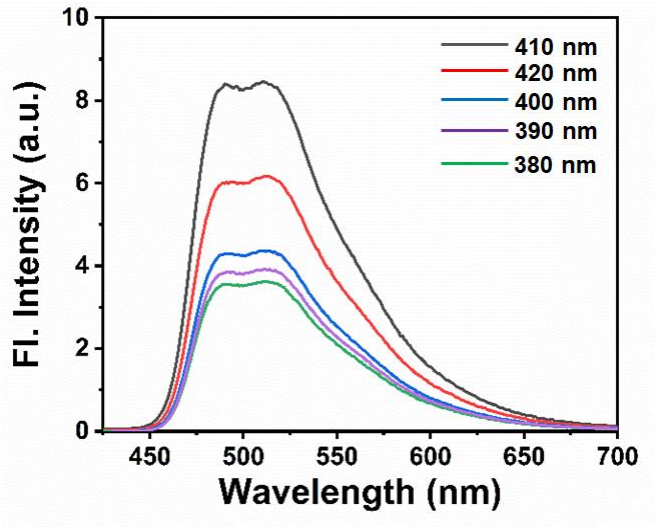

Fig. S4 Emission spectra of TPAn in THF (5 μM) with varying the λ_{ex} (380 to 420 nm at 10 nm interval).

Table S1. Spectroscopic data of TPAn in various polar solvents; the quantum yield, lifetime, and quality of fitting (χ^2) are shown.

Solvents	**Absorption**	**Emission**	**Quantum Yield**	**Lifetime (λ_{ex} = 407 nm)**	
Entry	**λ_{abs} (nm)**	**λ_{em} (nm)**	**%**	**τ (ns)**	**χ^2**
Toluene	422	484	18	0.6	1.15
		514		0.6	1.07
		548		0.6	1.12
THF	418	490	17	0.5	1.01
		511		0.5	1.16
DMF	419	523	13	0.4	1.19
DMSO	423	532	13	0.4	1.02

4.2. Absorption and emission measurements in the solid-state:

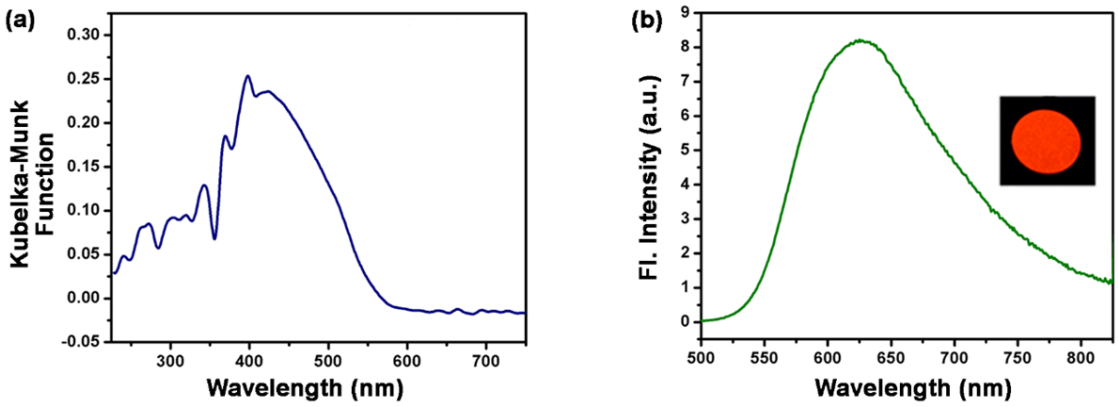

Fig. S5 Solid-state (a) absorption (using diffuse reflectance accessories [DRA] method), and (b) emission spectrum (λ_{ex} = 420 nm) of TPAn. Inset: the digital photograph of TPAn pellet under illumination at 365 nm.

4.3. Spectroscopic investigation of molecular aggregates

We used Milli Q water (resistivity: 18.2 MΩ. cm at 25 °C) for the aggregation studies. The pH of Milli Q water used was 6.98 ± 0.01 at 25 °C (Table S2, Fig. S6). The basic pyridine unit in TPAn is susceptible to acid. The pK_a of pristine pyridine is 5.2, and the pK_a of pyridine unit in 2-pyridylacetonitrile is between 3-4.[5,6] The protonation might have an impact on the nature of aggregation. Hence, we measured the pH of the binary solvent mixture of THF and water (Table S2, Fig. S6). It was in the range of 7.42 (10% water and 90% THF) and 6.98 (100% water). The pH of 80% water and 20% THF was found to be 6.99. Hence, in such a neutral and slightly basic medium, the protonation of the basic pyridine unit is not favourable.

Table S2. The pH of water-THF binary solvent mixtures with the variation of the composition at 25 °C (estimated pH range based on triplicate measurements).

System	pH at 25 °C
10% water – 90% THF	7.42 ± 0.02
20% water – 80% THF	7.42 ± 0.02
30% water – 70% THF	7.29 ± 0.02
40% water – 60% THF	7.18 ± 0.01
50% water – 50% THF	7.21 ± 0.01
60% water – 40% THF	7.08 ± 0.01
70% water – 30% THF	7.04 ± 0.02
80% water – 20% THF	6.99 ± 0.01
90% water – 10% THF	6.99 ± 0.01
100% water	6.98 ± 0.01

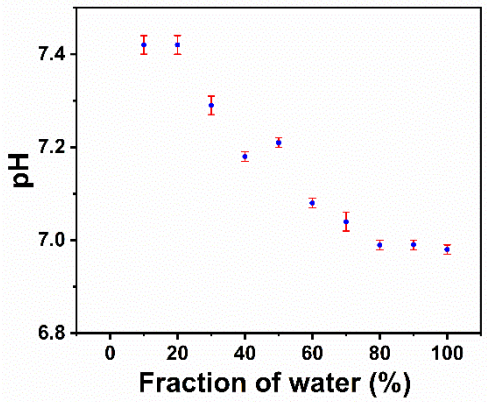

Fig. S6 The variation of pH vs. fraction of water (%) for the binary solvent mixtures of water and THF at 25 °C. The bars represent the standard deviations through triplicate measurements.

We measured the fluorescence quantum yields of TPAn dispersions in the binary solvent mixtures through the relative method using coumarin 153 as a fluorescent standard (eqn. no. S1).[1] A gradual decrease in the quantum yield was noticeable with increasing water content (Table S3, Fig. S7). It could be due to the activation of nonradiative decay channels induced by molecular aggregation.[7]

Table S3. Fluorescence quantum yield (FLQY) of TPAn dispersions in the binary solvent mixtures of water and THF with the composition variation. FLQY was estimated using coumarin 153 as the reference dye through triplicate measurements.

System	Quantum yield
TPAn in 10% water – 90% THF	8.37 ± 0.32
TPAn in 20% water – 80% THF	7.94 ± 0.29
TPAn in 30% water – 70% THF	7.07 ± 0.21
TPAn in 40% water – 60% THF	6.48 ± 0.30
TPAn in 50% water – 50% THF	5.92 ± 0.29
TPAn in 60% water – 40% THF	5.65 ± 0.35
TPAn in 70% water – 30% THF	4.32 ± 0.29
TPAn in 80% water – 20% THF	3.71 ± 0.26
TPAn in 90% water – 10% THF	2.15 ± 0.35

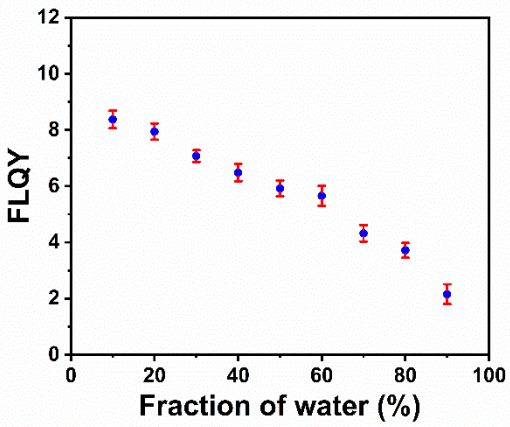

Fig. S7 Fluorescence quantum yield (FLQY) vs. fraction of water (%) plot for TPAn dispersions. The bars represent the standard deviations through three independent measurements.

V. Microscopic and FCS analysis of aggregates

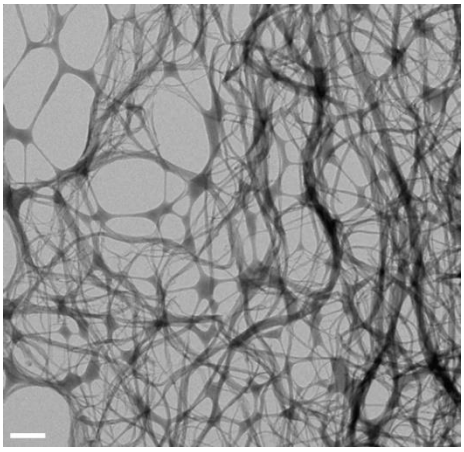

Fig. S8 TEM image of TPAn aggregates [THF (20%) - water (80%)]. Scale = 1 μm.

Samples for the electron microscopy were prepared by drop-casting the as-prepared dispersion. The TEM image of the TPAn aggregates [THF (20%) - water (80%)] showed the connected network of the nanofibers (Fig. S8). The dimension of the nanostructures (the network of nanofibers, Fig. 2f, 2g, S8) was much higher in the solvent-evaporated samples compared to that obtained in the dispersion through FCS, which we attributed to the drying effects. The 80% aqueous dispersion was further diluted with water to rule out the possibility of aggregation due to the higher concentration of the dispersion. However, both the AFM and FESEM images of the diluted samples also showed a similar kind of connected network of the nanofibers rather than smaller nanofibers probed through FCS in the dispersion (Fig. S9, S10). The results implied that the dilution could not inhibit the drying effect during the solvent evaporation.

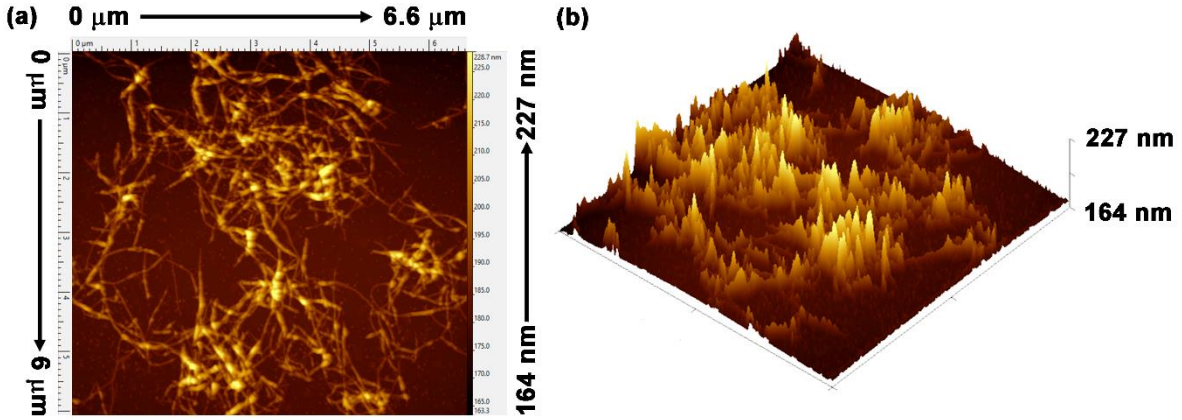

Fig. S9 Topographic atomic force microscopy images of pristine aggregates [THF (20%) - water (80%)]: (a) along the X-Y plane and (b) the Z-axis; as prepared dispersion was further diluted with water for sample preparation.

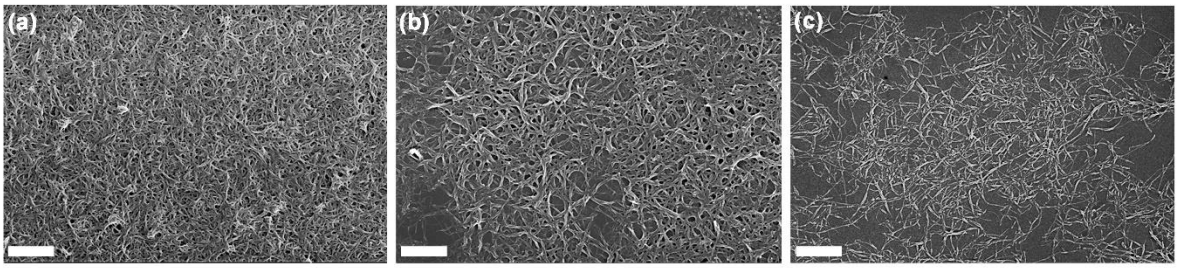

Fig. S10 FESEM images of TPAn aggregates [THF (20%) - water (80%)]: (a) as prepared dispersion, (b, c) gradual dilution of the dispersion during sample preparation with water suggesting network of nanofibers. Scale = 1 μm.

The autocorrelation function G(τ) is defined as,

$$G(\tau) = \frac{<\delta F(0)\ \delta F(\tau)>}{<F>^2} \ldots\ldots\ldots (S3)$$

where, F(0) and F(τ) indicate the fluorescence intensity at time 0 and at a lag time τ around the mean value, respectively.[1,8,9] To ensure the absence of free TPAn molecule in dispersion having 80% water content, we filtered the same using a nanoporous Whatman disc (Anodisc, pore size 0.02 μm). No emission from the supernatant confirmed the absence of free TPAn molecules in the dispersion (Fig. S11). On the other hand, the fitting of the correlation functions for the samples with 50-70% water fraction and the reversible morphological transformation in the presence of acid and base were carried out with the two-component diffusion model considering TPAn molecules both in solution and in the form of aggregates (eqn. no. S4; Fig. S12).[10] The fitting of the FCS traces of TPAn in THF, THF-water mixture with 80% water, and inside HeLa cells were carried out using the three-dimensional (3D) diffusion model (eqn. no. S5).[10]

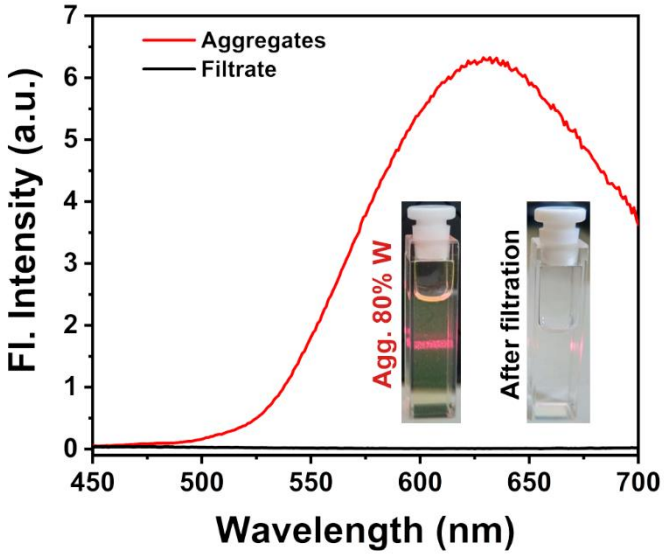

Fig. S11 Emission spectra of TPAn dispersion (30 μL, 0.2 mM TPAn stock solution in 3 mL THF-water mixture with 80% water content) and the supernatant obtained through the filtration of the dispersion using a nanoporous Whatman disc (Anodisc, pore size 0.02 μm). Inset: the digital photographs of dispersion and the true solution after the filtration in the presence of red laser light.

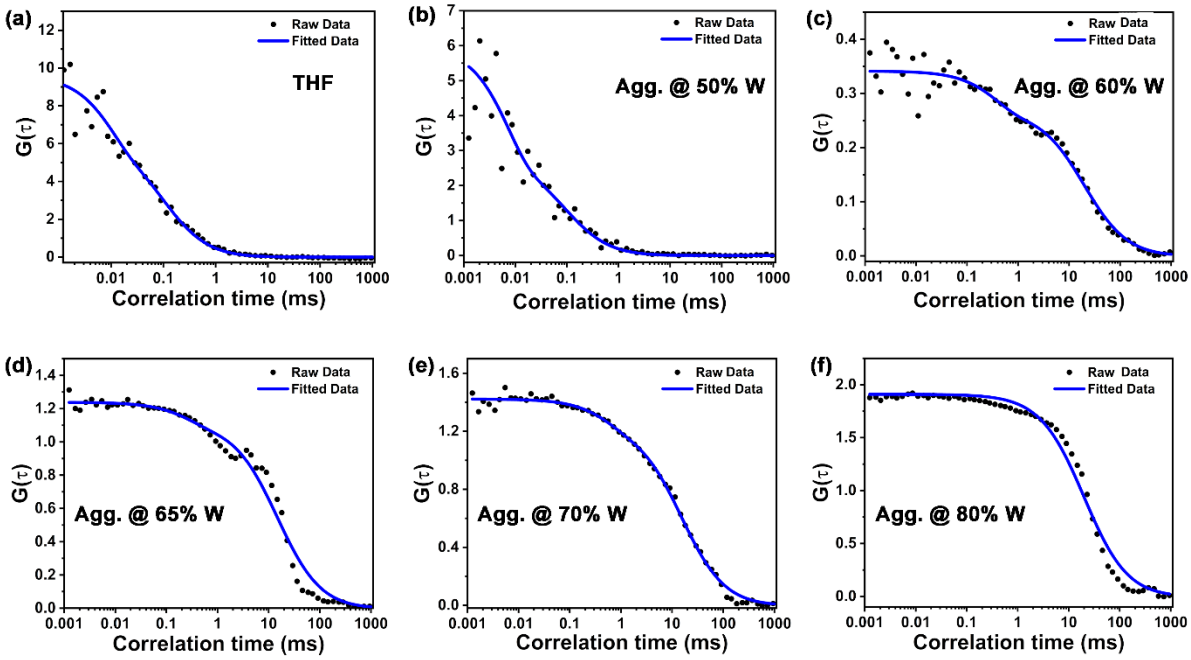

Fig. S12 Raw and corresponding fitted FCS traces for TPAn (a) in THF, and (b-f) in the form of aggregates varying the water content (W).

$$G(\tau) = \frac{1}{N}\left[\left[\frac{1-y}{\left(1+\frac{\tau}{\tau_{D1}}\right)}\frac{1}{\sqrt{1+\frac{\tau}{\omega^2\tau_{D1}}}}\right] + \left[\frac{y}{\left(1+\frac{\tau}{\tau_{D2}}\right)}\frac{1}{\sqrt{1+\frac{\tau}{\omega^2\tau_{D2}}}}\right]\right] \quad \text{.....(S4)}$$

$$G_{3D}(\tau) = \frac{1}{N}\frac{1}{1+\frac{\tau}{\tau_D}}\frac{1}{\sqrt{1+\frac{\tau}{\omega^2\tau_D}}} \quad \text{.....(S5)}$$

$G(\tau)$ is the autocorrelation function, N is the average number of fluorescent particles in the detection volume, τ_D is the diffusion time, τ is the correlation time, τ_{D_1} and τ_{D_2} are the diffusion time of free and aggregated TPAn molecules, respectively, and y is the fraction of aggregated TPAn molecules. ω is the structural parameter of the 3D Gaussian confocal volume, defined as $\omega = \omega_z/\omega_{xy}$, where ω_z is the longitudinal radius, and ω_{xy} is the transverse radius of the focal volume. Standard rhodamine 6G solution in water (D_t = 426 μm^2 s^{-1}) was used to calibrate the

Table S4. Tabular representation of diffusion time (τ_D), total diffusion coefficient (D_t), and the size parameters of TPAn nanostructures obtained through FESEM and FCS measurements. The standard deviations of diffusion time and total diffusion coefficient were estimated using the data from three independent measurements.

System	τ_D (ms)	D_t (μm^2 s^{-1})	Diameter (nm) FESEM	Length (μm) FCS
THF	0.10 ± 0.02	194 ± 49.70	-----	-----
70% W	10.45 ± 1.03	1.83 ± 0.13	40	-----
80% W	33.70 ± 1.90	0.57 ± 0.02	60	0.40 ± 0.02

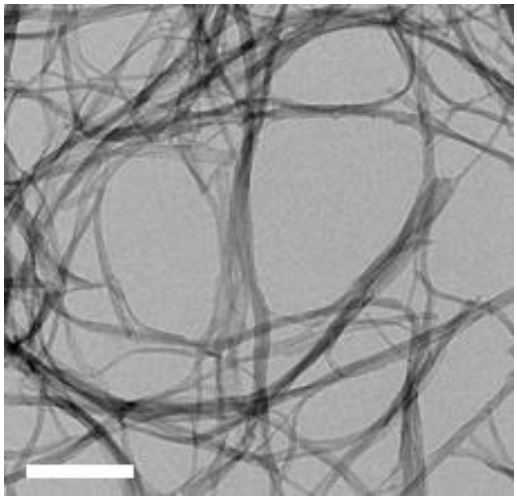

Fig. S13 HRTEM image of the TPAn aggregates having water fraction of 99% (scale = 200 nm).

value of ω and the same was found to be 5.[11] For 50 μm pinhole ω_{xy} was found to be ~270 nm. The confocal volume of the setup was ~ 0.55 fL. IgorPro 6 software was used to analyze the acquired data. The total diffusion coefficient (D_t) was estimated through the eqn. no. S6 using the value of ω_{xy} and diffusion time (τ_D). The τ_D, D_t, and size parameters of TPAn in the form of a molecule and molecular aggregates are summarized in Table S4.

$$D_t = \frac{\omega_{xy}^2}{4\tau_D} \text{.....(S6)}$$

$$R_h = \frac{k_B T}{6\pi\eta D_t} \text{.....(S7)}$$

The hydrodynamic radius of the spherical nanoparticles can be calculated using the Stokes-Einstein equation (eqn. no. S7). Here, R_h is the hydrodynamic radius of the nanoparticles, k_B is Boltzmann's constant, T is the temperature, η is the viscosity of the solvent, and D_t is the total diffusion coefficient. However, the Stokes-Einstein equation is not valid for anisotropic nanofibers (80% water fraction). Hence, the Stick hydrodynamic boundary condition was applied to modify the Stokes-Einstein equation (eqn. no. S8-S10).[12,13]

$$D_{\parallel} = \frac{k_B T}{2\pi\eta L} \ln\left(L/d\right) \text{.....(S8)}$$

$$D_{\perp} = \frac{k_B T}{4\pi\eta L} \ln\left(L/d\right) \text{.....(S9)}$$

$$D_t = (D_{\parallel} + 2D_{\perp})/3 \text{.....(S10)}$$

According to Stick's theory for rod-like particles, the diffusion coefficient parallel to the major axis ($D_{\parallel}$) is double that of the minor axis ($D_{\perp}$) (eqn. no. S10). L and d, are respectively the length and diameter of the fibers. The value of d was taken in between a range of 20 to 120 nm after the close inspection of the electron microscopy images. Eqn. no. S8-S10 were solved using Newton-Raphson method and the average length of the nanofibers in the dispersion with 80% water content was found to be ~ 0.4 μm.

VI. Impact of solvent polarity

6.1. TPAn aggregates in DMSO-water and THF-hexane binary solvent mixture:

The spectroscopic investigation for TPAn was carried out in DMSO-water binary solvent mixture to understand the impact of solvent polarity on the aggregation behavior. No significant changes were observed in the absorption and emission of TPAn with increasing water fractions up to 30%. However, the drastic change in both the absorption and emission spectra was noticeable from 40% water fraction onwards (Fig. S14a, S14b). The plot of the extent of aggregation against the fraction of water revealed the steep rise at 30-40% water fraction, signifying it as the most effective regime of TPAn aggregation in DMSO-water solvent mixture (Fig. S14c). The FESEM image showed the formation of nanofiber for the dispersion having 60% DMSO and 40% water fraction (ε ~ 64) similar to the THF-water mixture having the water fraction 80% (ε ~ 60; Fig. S14d).[14] The morphology of TPAn aggregates was also checked in THF-hexane binary solvent mixture having 20% THF and 80% hexane content to understand the role of water. However, at similar conditions, unlike nanofibers, we observed the formation of spherical nanoaggregates (Fig. S15).

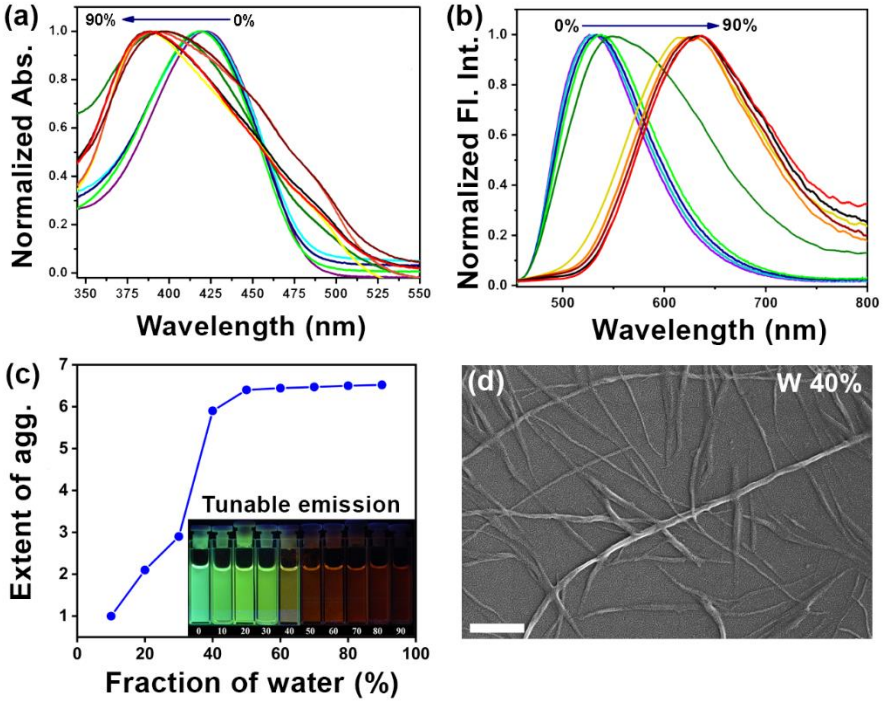

Fig. S14 Normalized (a) absorption and (b) fluorescence emission spectra (excited at individual λ_{max}^{abs}) of TPAn (30 μL, 0.2 mM TPAn stock solution in 3 mL DMSO-water mixture) with varying the water fraction from 0 to 90%. (c) The plot of the extent of aggregation against the fraction of water depicting self-assembly of TPAn induced by increasing content of 'bad solvent', water. Inset: the digital photographs of aqueous dispersions of TPAn under the UV light irradiation (λ_{ex} = 365 nm). (d) FESEM image of the self-assembled aggregates of TPAn in DMSO-water mixture having the water content of 40%. Scale = 200 nm.

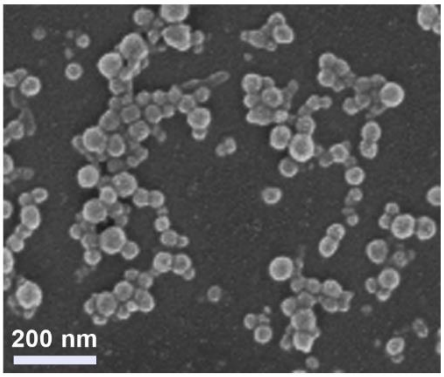

Fig. S15 FESEM image of the self-assembled aggregates of TPAn in THF-hexane mixture having the hexane content of 80%. Scale = 200 nm.

VII. Role of pyridinic nitrogen

7.1. FCS analysis for reversible morphological transformation:

The reversible morphological transformation in the presence of acid and base was also monitored through FCS analysis (Fig. S16). As the presence of both free and aggregated TPAn was possible during the course of morphological transformation; hence, we fitted the raw FCS traces using the two-component diffusion model (eqn. no. S4). The normalized FCS traces demonstrated the transformation of pristine nanofibers to nanoparticles and *vice versa* with time due to the protonation and deprotonation of the pyridinic nitrogen center upon the addition of acid and base, respectively (Fig. 4h, Fig. S16, S17).

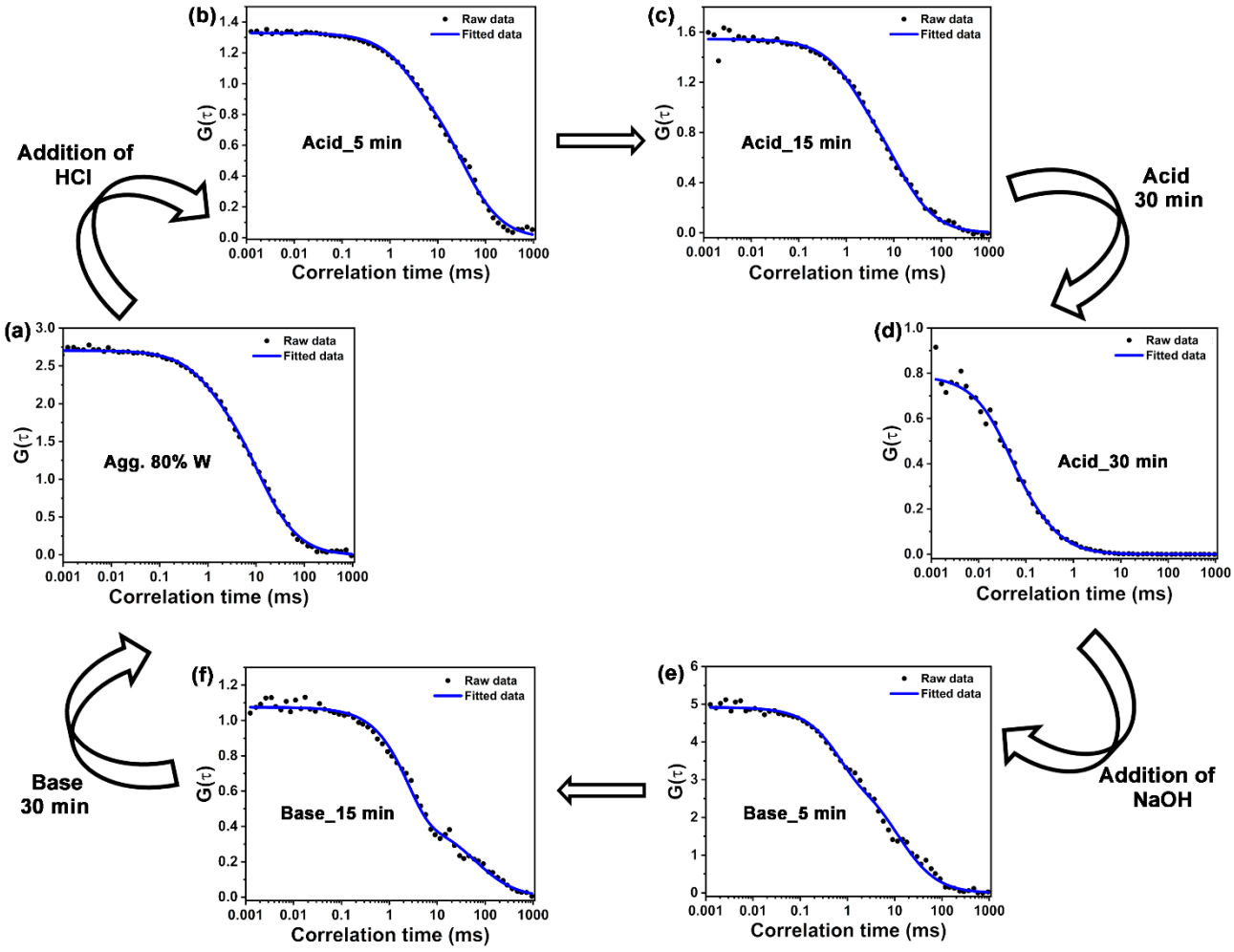

Fig. S16 Raw and corresponding fitted FCS traces depicting the morphological transformation of TPAn nanofibers (80% water-20% THF) to a solution-like signature (dissolution of nanofibers to smaller sized nanoparticles) and *vice versa* with time upon addition of 50 μL, 11.1 (M) HCl, and 50 μL, 11.1 (M) NaOH, respectively.

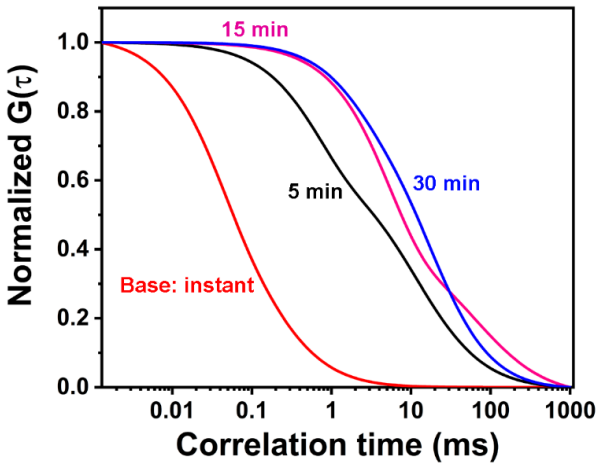

Fig. S17 Normalized best fit FCS traces depicting the reformation of nanofibers from nanoparticles due to the addition of base [50 μL, 11.1 (M) NaOH] into the acidified dispersion of TPAn.

We also monitored the aggregation behaviour of TPAn in 80% water – 20% THF mixture with the variation of pH of the medium. For the medium with pH 8, 7, and 4, no change in emission spectra for the nanofiber dispersion was observed even after one hour (Fig. S18). In contrast, for pH 3, 2.5, and 1.5, the emission peak intensity at ~ 630 nm decreased with a concomitant increase in emission peak intensity at ~ 500 nm with time (Fig. S18). Additionally, it was found that less time was required for the transformation from the network of nanofibers to nanoparticles for the samples having pH ~ 0.7 and 1.5 (30 min) as compared to that of pH ~ 2.5 (90 min) and pH ~ 3 (105 min). The spectroscopic observations of the disintegration of supramolecular nanofibers were also supported by FESEM studies (Fig. S19). The results

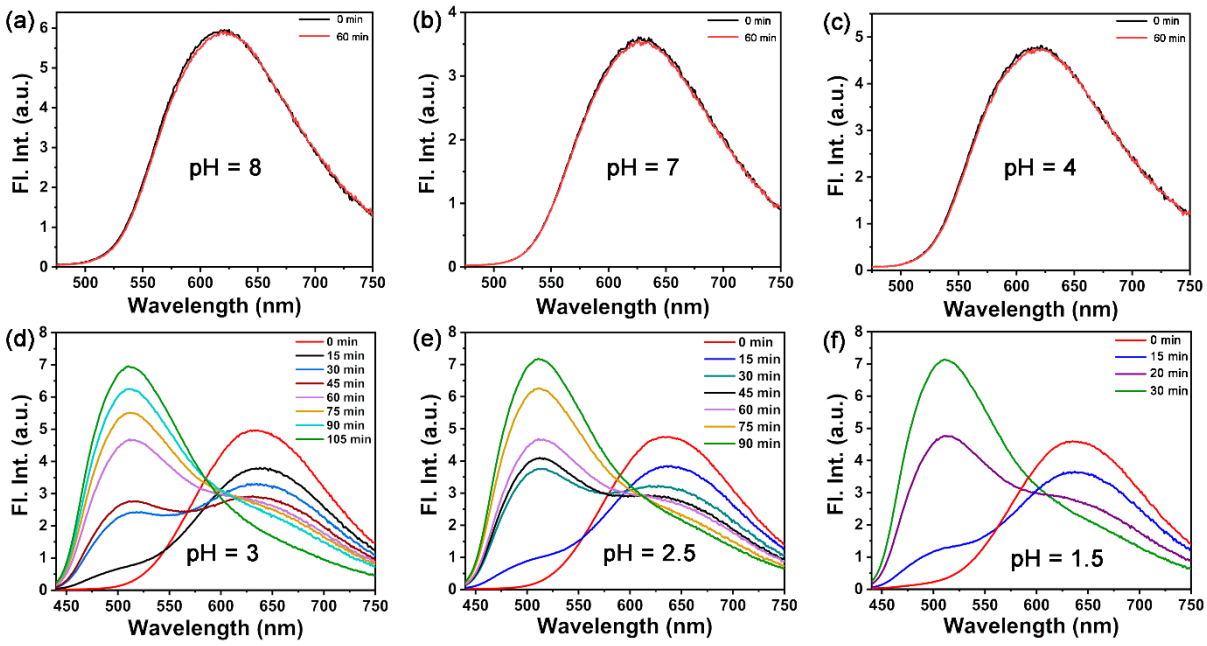

Fig. S18 Steady-state emission spectra of TPAn dispersion (80% water-20% THF) having the pH of the medium (a) 8, (b) 7, (c) 4, (d) 3, (e) 2.5, and (f) 1.5 at different time intervals.

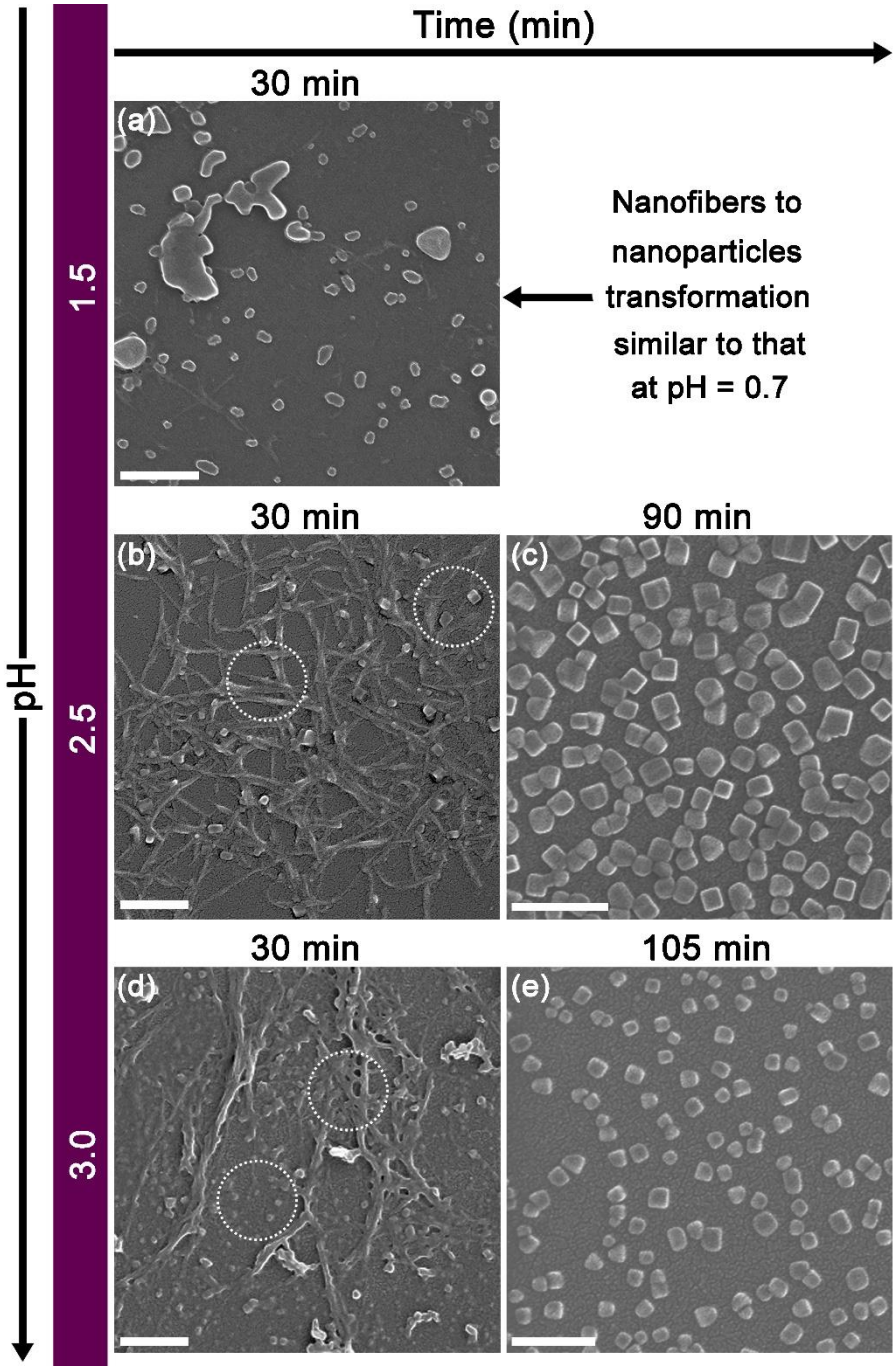

Fig. S19 Field emission scanning electron microscopy (FESEM) images of TPAn dispersion (80% water-20% THF) having the pH of the medium 1.5, 2.5, and 3 at different time intervals. (a) FESEM image of the dispersion having pH ~ 1.5 after 30 min of the acid addition. (b, c) FESEM images of the dispersion having pH ~ 2.5 after 30 min and 90 min of the acid addition. (d, e) FESEM images of the dispersion having pH ~ 3 after 30 min and 105 min of the acid addition. Scale = 200 nm.

obtained at different pH qualitatively revealed that the protonation of TPAn could only take place in a highly acidic medium.

7.2. Molecular modelling:

TPAn dispersion having a water content of 80% was centrifuged, and the obtained residue was used to get the PXRD data. Fig. S20a demonstrates the PXRD patterns of TPAn aggregates. The sharp peaks in the PXRD data confirmed the highly crystalline nature of TPAn. The unit cell dimensions were first determined by the observed powder X-ray diffraction peak positions using the reflex module (a software package implemented in Material Studio 6.1). Further, the unit cell parameters were refined by the Pawley method constructed until the (R_{wp}) value converged. The refinement provided the unit cell with the cell parameters of a = 14.6 Å, b = 12.5 Å, c = 6.9 Å, and $\alpha = \beta = \gamma = 90°$ with R_{WP} = 0.21%. Each unit cell contains four TPAn molecules having no intermolecular interactions (Fig. S20b). However, the intermolecular interactions between the molecules of two adjacent unit cells resulted in the formation of 3D supramolecular self-assembly with anisotropic architecture (Fig. S20c, Fig. 5c, 5d).

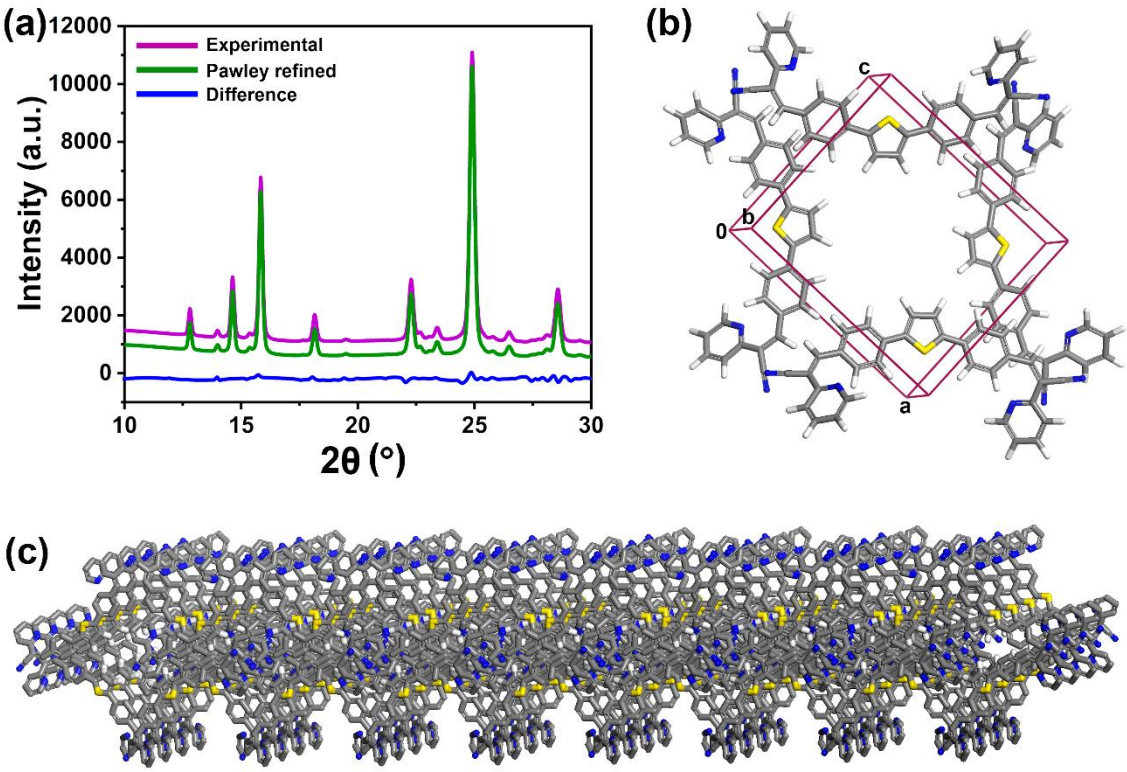

Fig. S20 (a) Powder X-ray diffraction (PXRD) patterns of TPAn: comparison between the experimental pattern (magenta), Pawley refined profile (green), and the refinement differences (blue). (b) The unit cell was obtained through the Pawley refinement of the experimental PXRD pattern using the Materials Studio 6.1 package. (c) Three-dimensional (3D) supramolecular assembly of TPAn depicting the formation of anisotropic structure. Color code: C = grey, H = white, N = blue, and S = yellow; hydrogen atoms are omitted for clarity except those involved in noncovalent interactions.

7.3. Spectroscopic and microscopic investigation of TPAnWN:

To get the more insight into the role of pyridinic nitrogen centers of TPAn on the self-assembly process, a new compound TPAnWN (without pyridinic nitrogen centers) was synthesized (Fig. S21a). TPAnWN dispersion in THF-water mixture having the 80% fraction of water showed a cuboid morphology as revealed from the FESEM and HRTEM images (Fig. S21b). No change in the emission spectra was observed for TPAnWN aggregates upon the addition of acid (Fig. S21c, S21d).

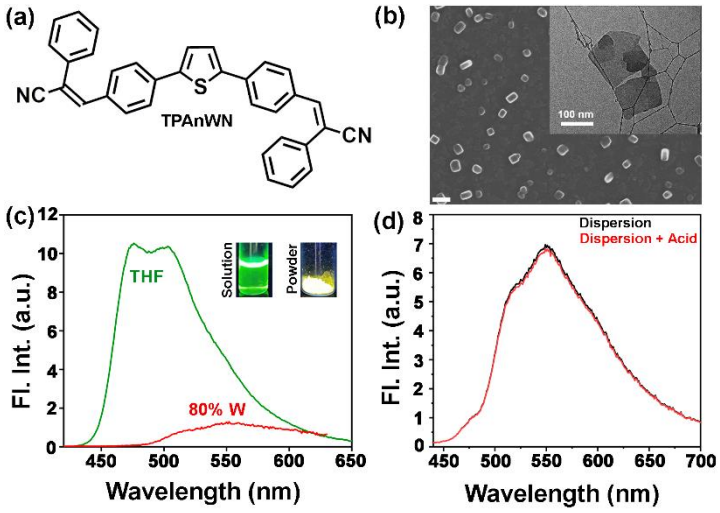

Fig. S21 (a) Chemical structure of TPAnWN. (b) The FESEM image of TPAnWN aggregates in THF-water mixture with 80% water content illustrating a cuboid morphology. Inset: HRTEM image of TPAnWN aggregates. Scale = 100 nm. (c) Emission spectra (λ_{ex} = 410 nm) of TPAnWN in THF (5 μM) and TPAnWN (0.2 mM, 30 μL) in 3 mL THF-water mixture having the water fraction 80%; inset: the digital photographs showing green and yellowish-orange fluorescence of TPAnWN in the form of solution and powder, respectively under the illumination at 365 nm. (d) Emission spectra of TPAnWN dispersion (80% water fraction) before and after the addition of 50 μL, 11. 1 (M) HCl (pH of 3.08 mL dispersion ~ 0.7).

VIII. Probing microenvironments

TPAn might internalize to the lipid-enriched organelles, such as lipid droplets (LDs), due to the hydrophobic interactions. Hence, HeLa cells were first incubated with 30 nM of TPAn and then with 30 nM of Nile red (commercial LD-tracker) for 30 min (Fig. 7). Additionally, we also carried out the colocalization experiments with lysotracker deep red (LTDR) and mitotracker red (MTR). The results showed lower PCC values of 0.42 and 0.53 for TPAn with LTDR and MTR, indicating no specific internalization of TPAn in lysosome and mitochondria, respectively (Fig. S22, S23).

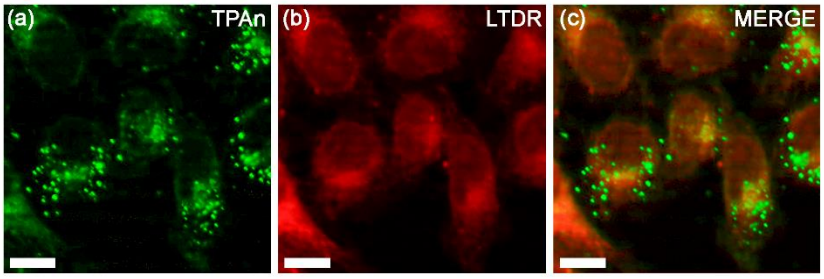

Fig. S22 Fluorescence microscopy images of HeLa cells costained with TPAn (30 nM) and lysotracker deep red (30 nM): using (a) a GFP filter (green channel, λ_{ex} = 450-490 nm, λ_{em} = 500-550 nm), and (b) a DsRed filter (red channel, λ_{ex} = 538-562 nm, λ_{em} = 570-640 nm). (c) Merged fluorescence image depicting cellular staining by TPAn and lysotracker deep red. Scale = 20 µm.

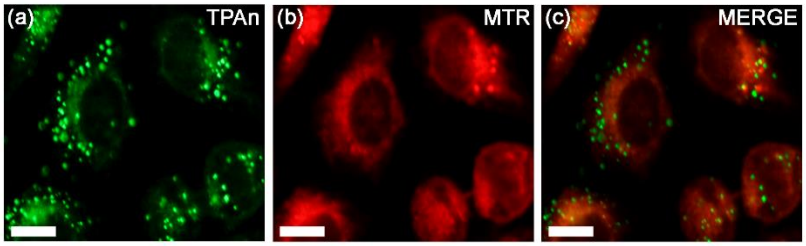

Fig. S23 Fluorescence microscopy images of HeLa cells costained with TPAn (30 nM) and mitotracker red (30 nM): using (a) a GFP filter (green channel, λ_{ex} = 450-490 nm, λ_{em} = 500-550 nm), and (b) a DsRed filter (red channel, λ_{ex} = 538-562 nm, λ_{em} = 570-640 nm). (c) Merged fluorescence image depicting cellular staining by TPAn and mitotracker red. Scale = 20 µm.

As lipid is one of the major components of the cell membrane, the staining of the lipidic component present in the cell membrane by TPAn cannot be ruled out. We further carried out confocal laser scanning microscopy (CLSM) imaging of HeLa cells costained with TPAn and cellmask deep red (CMDP; tracker for the cell membrane) dyes. The colocalization images showed the possible staining of the lipidic component in the cell membrane by TPAn in addition to distinct imaging of lipid droplets (Fig. S24).

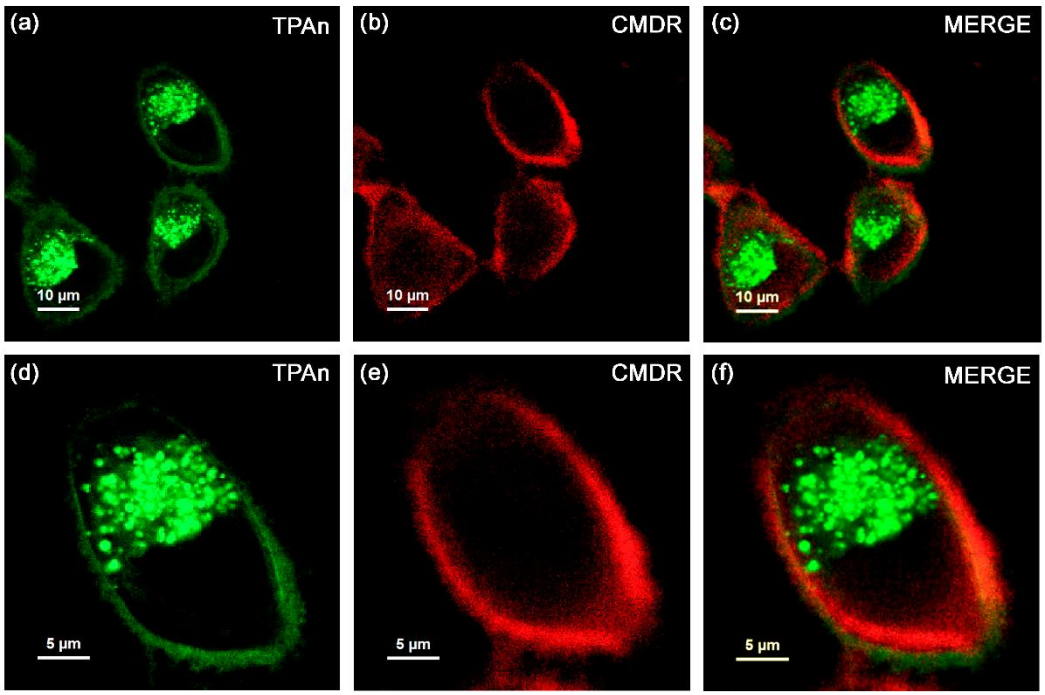

Fig. S24 Confocal laser scanning microscopy (CLSM) images of HeLa cells costained with TPAn (30 nM) and cellmask deep red (CMDR; 30 nM) for 15 mins. (a) Cell imaging using TPAn, and (d) the zoom view of the same image (λ_{ex} = 405 nm, λ_{em} = 425-532 nm). (b) Staining of the cell membrane by CMDR, and (e) the zoom view of the same image (λ_{ex} = 640 nm, λ_{em} = 650-800 nm). (c, f) The merged images of TPAn and CMDR depicting the internalization of TPAn toward the lipidic component of cell membrane along with distinct localization in LDs. Scale: (a-c) = 10 μm and (d-f) = 5 μm.

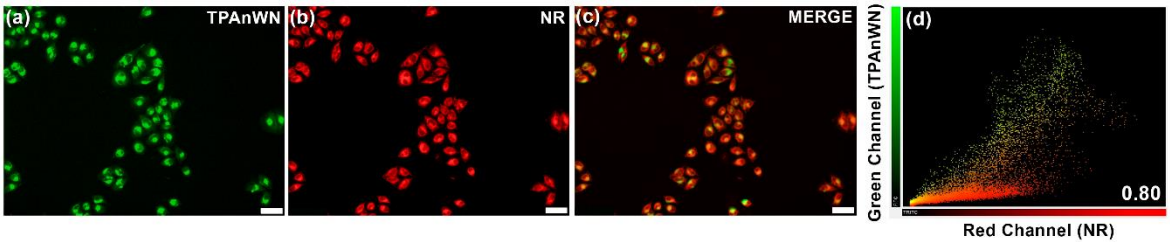

Fig. S25 Fluorescence microscopy images of HeLa cells costained with TPAnWN (20 μM) and Nile red (30 nM): using (a) a GFP filter (green channel, λ_{ex} = 450-490 nm, λ_{em} = 500-550 nm), and (b) a DsRed filter (red channel, λ_{ex} = 538-562 nm, λ_{em} = 570-640 nm). (c) Merged fluorescence image of TPAnWN and Nile red depicting colocalization in LDs, and (d) Pearson's correlation of TPAnWN and Nile red intensities (correlation coefficient: 0.80). Scale (a-c) = 50 μm.

In addition, we performed the internalization of TPAnWN in HeLa cells. The solubility and quantum yield (QY) of TPAnWN in DMSO (QY: 5 %) were much lower than TPAn (QY: 13%). We found that 20 μM was the minimum concentration required to get the cellular images using TPAnWN (unlike nM concentration for TPAn). However, the higher content of DMSO in such concentration led to cell death. Hence, live cell imaging with TPAnWN was not possible. In order to compare the cellular internalization, we fixed the HeLa cells and performed the colocalization study with Nile red. TPAnWN could also stain the lipid droplets with a lower PCC value of 0.80 as compared to TPAn (PCC: 0.90; Fig. S25, Fig. 7).

Expansion and shrinkage of LDs play a vital role in cellular metabolism.[15] Such dynamic nature of LDs is significantly affected by the local polarity and viscosity of the environment.[16,17] To monitor the emission behavior of TPAn inside the HeLa cells, we chose a particular region of the confocal image and recorded the spectrum (Fig. S26). The emission spectrum of TPAn inside the cells (λ_{em} = 470 nm) was quite similar to that in the nonpolar solvent like toluene (Fig. S26). Thus, the polarity of LDs in HeLa cells resembled that of toluene (dielectric constant: $\varepsilon \sim 2.5$).

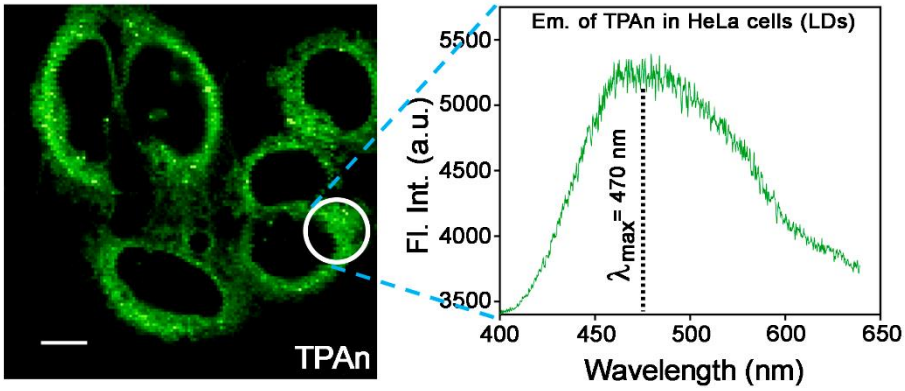

Fig. S26 Confocal laser scanning microscopy (CLSM) image of live HeLa cells incubated for 15 mins with 30 nM TPAn (λ_{ex} = 405 nm, λ_{em} = 425-800 nm). Scale = 10 μm. The emission spectrum of TPAn (30 nM) at the region of interest inside HeLa cells.

Probing the viscosity in lipid droplets (LDs):

The total diffusion time of TPAn inside the HeLa cell was obtained from the fitted FCS traces using the eqn. no. S5 (Fig. S27). Viscosity in lipid droplets was calculated using the eqn. no. S11. τ_{THF} and τ_{Cell} are the total diffusion time of TPAn in THF and HeLa cells, respectively. η_{THF} and η_{Cell} are the viscosity sensed by TPAn in THF and HeLa cells, respectively.

$$\frac{\tau_{\mathrm{THF}}}{\tau_{\mathrm{Cell}}} = \frac{\eta_{\mathrm{THF}}}{\eta_{\mathrm{Cell}}} \ldots\ldots\ldots (S11)$$

where, τ_{THF} = 0.1 ms, τ_{Cell} = 9 ms (Fig. 7f), and η_{THF} = 0.48 cP at 25 °C.[18]

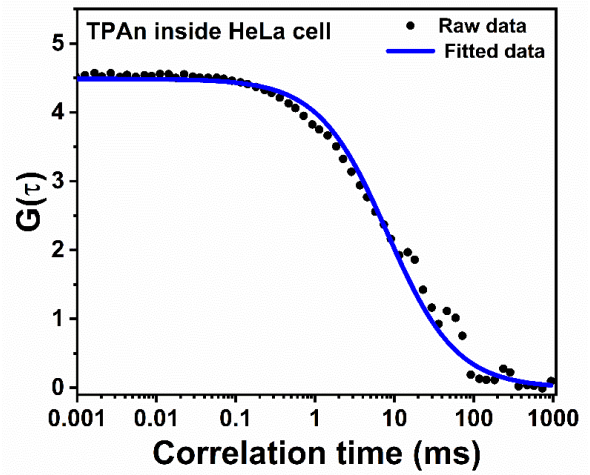

Fig. S27 Raw and corresponding fitted FCS traces of TPAn (30 nM) inside the HeLa cells.

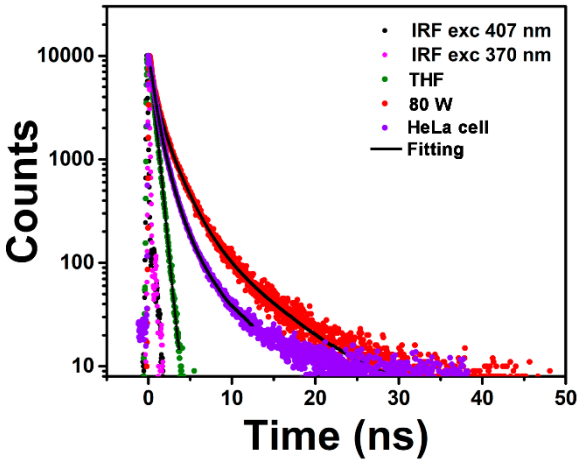

Fig. S28 Emission decay profiles of TPAn in THF (green; λ_{ex} = 410 nm, λ_{em} = 525 nm), lipid droplets (violet, λ_{ex} = 405 nm, λ_{em} = 475 nm) and in THF-water solvent mixture having water content 80% (red; λ_{ex} = 370 nm, λ_{em} = 630 nm).

IX. ^{1}H, and ^{13}C NMR Spectra

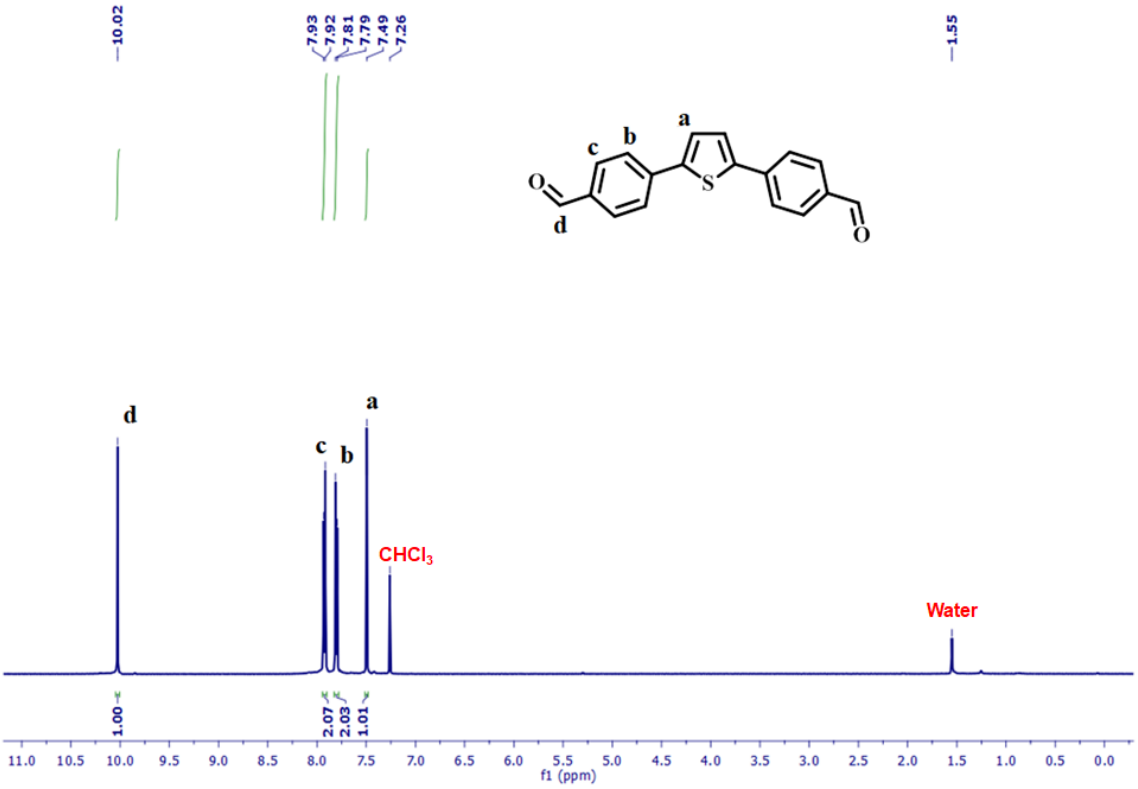

Fig. S29 ^{1}H NMR (500 MHz) spectrum of TBA in $CDCl_3$ at room temperature.

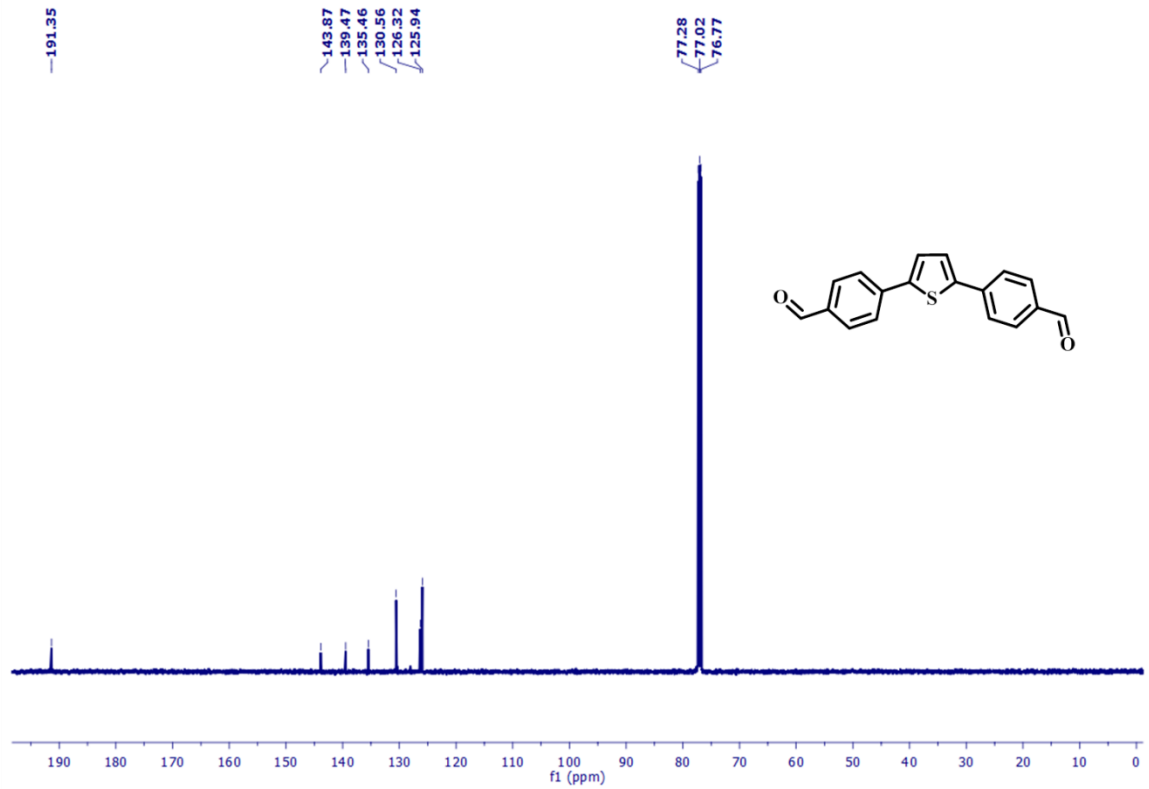

Fig. S30 ^{13}C NMR (126 MHz) spectrum of TBA in $CDCl_3$ at room temperature.

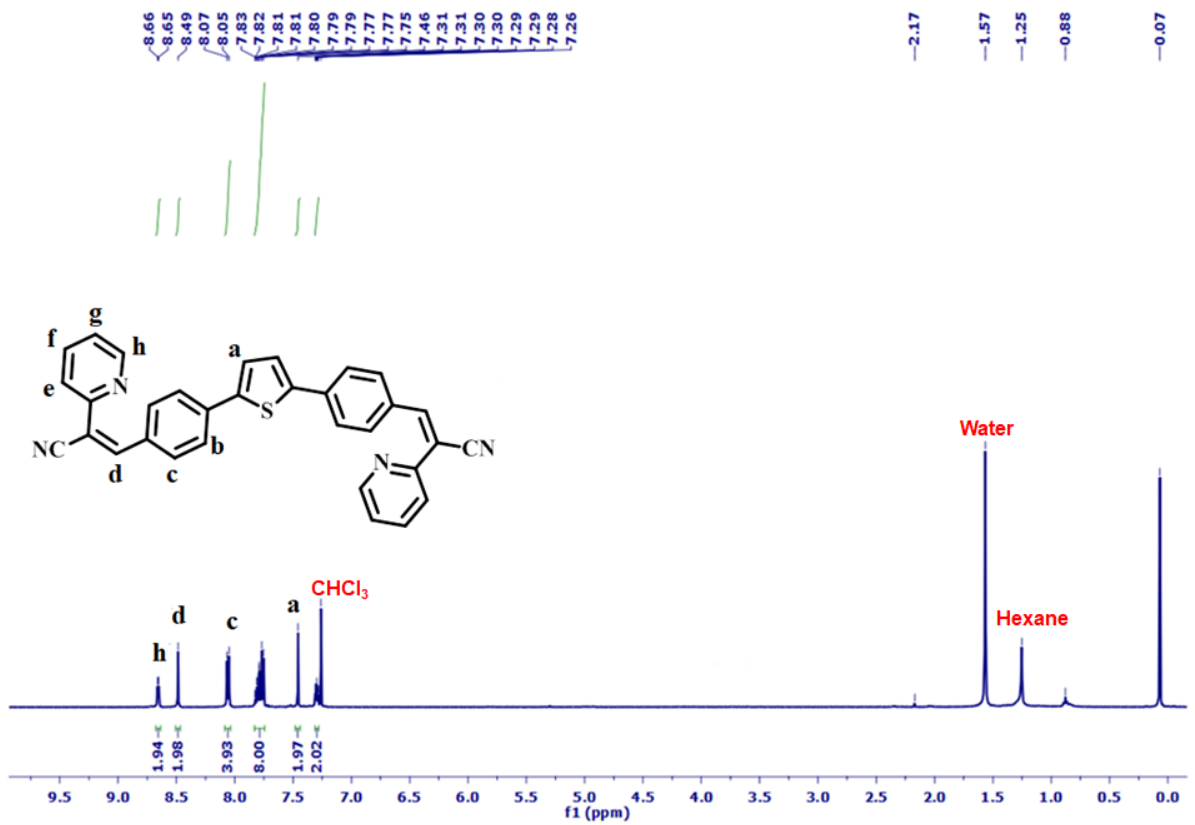

Fig. S31 ^{1}H NMR (500 MHz) spectrum of TPAn in $CDCl_3$ at room temperature.

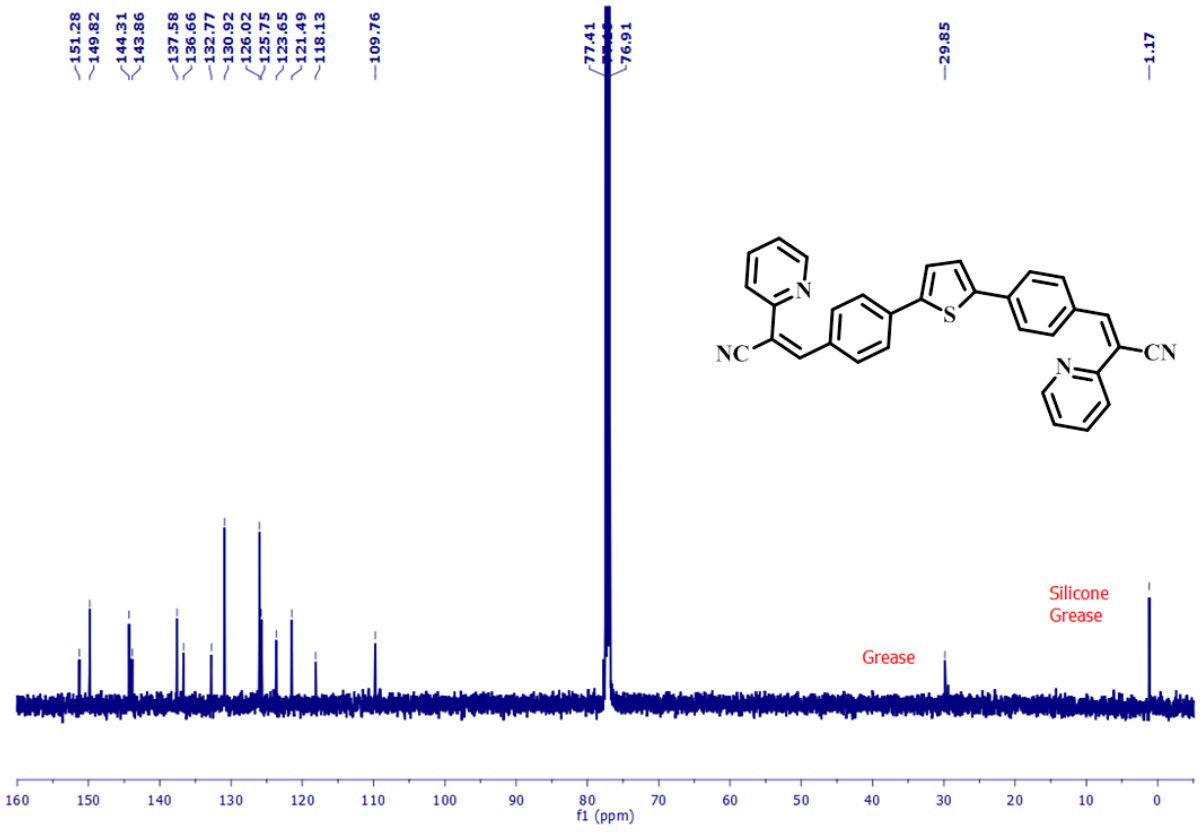

Fig. S32 ^{13}C NMR (126 MHz) spectrum of TPAn in $CDCl_3$ at room temperature.

Nuclear overhauser effect spectroscopy (NOESY) analysis:

We wanted to get more insight into the spatial arrangement of -CN units in TPAn. However, we could not perform the two-dimensional nuclear magnetic resonance spectroscopy (2D NMR) due to the low solubility of TPAn. We performed the nuclear overhauser effect spectroscopy (NOESY) analysis. When a nucleus is spatially close to another nucleus, a change in the integrated resonance intensity of the NMR peak of the first nucleus occurs when another is saturated by an irradiation of a radio frequency (RF) pulse and *vice versa*.[19] We identified four protons of TPAn comparing with the ^{1}H NMR spectrum of TBA. We could interpret that the 'e' type proton belonged to the multiplet region. As we expect a symmetric TPAn molecule (singlet peak at 7.46 ppm for thiophene unit), either the "E, E" or "Z, Z" configuration is possible. For a Z-type configuration, 'd' and 'e' protons are spatially coupled, which is not true for the E-type configuration (Fig. S33). When irradiated at 8.50 ppm for the 'd' proton, we did not notice any change in the multiplet region. Similarly, when irradiated at the multiplet region, no prominent variation in the peak at 8.50 ppm for 'd' proton was noticeable. Hence, we could conclude the E, E configuration of TPAn (Fig. S33).

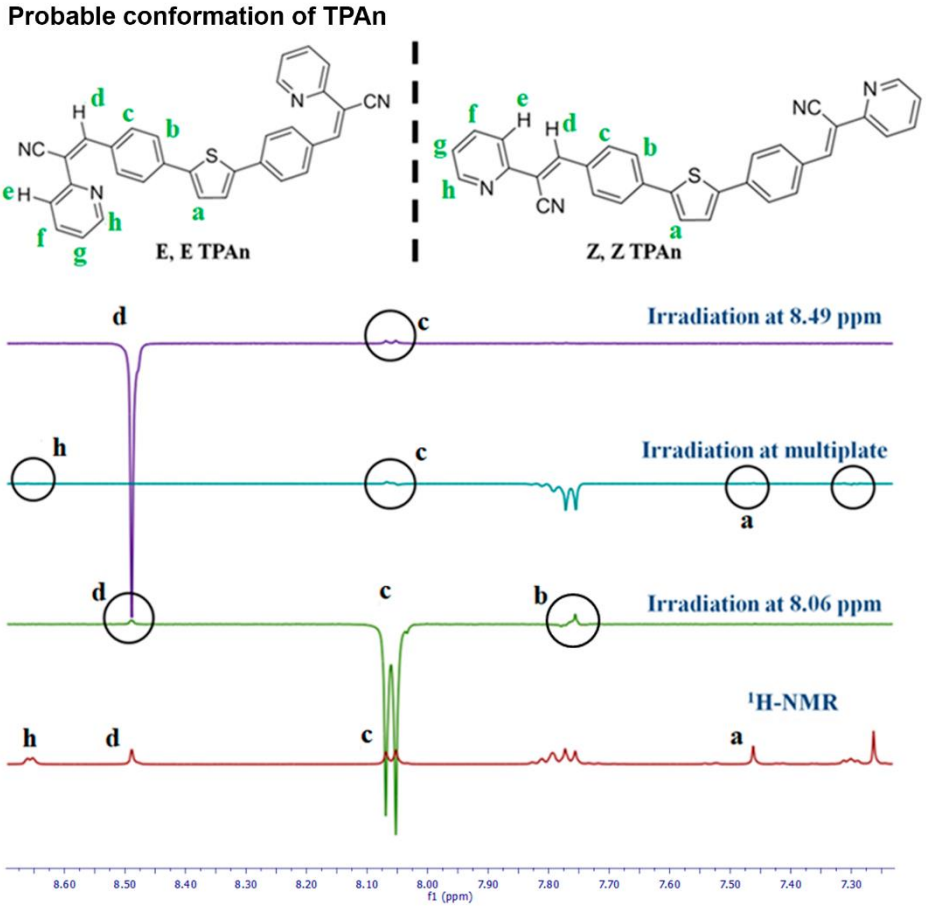

Fig. S33 Possible configurations of TPAn (up) and NOE (^{1}H NMR) spectrum of TPAn in $CDCl_3$ (bottom). The analysis suggests (E, E) configuration for TPAn.

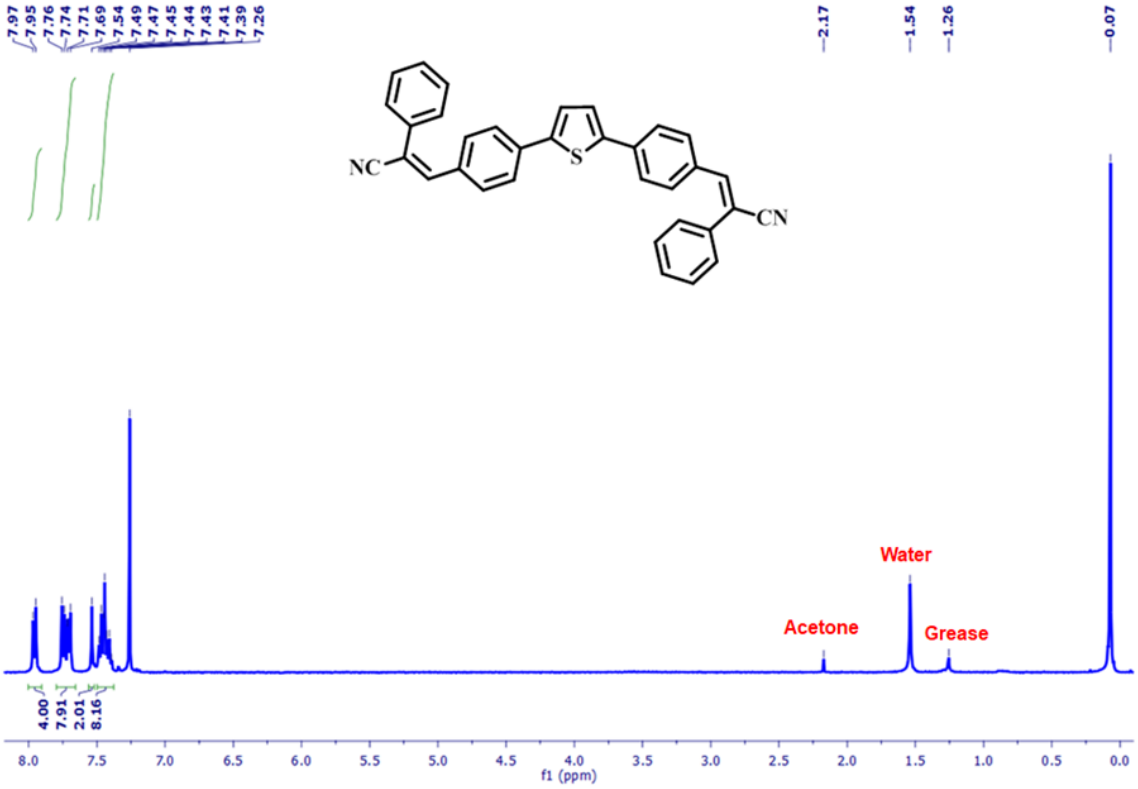

Fig. S34 ^{1}H NMR (400 MHz) spectrum of TPAnWN in $CDCl_3$ at room temperature.

X. References

1. J. R. Lakowicz, *Principles of Fluorescence Spectroscopy*, Springer, New York, 2006.

2. S. Chakraborty, S. Nandi, K. Bhattacharyya and S. Mukherjee, *ChemPhysChem*, 2020, **21**, 406.

3. K. Guo, F. Zhang, S. Guo, K. Li, X. Lu, J. Li, H. Wang, J. Cheng and Q. Zhao, *Chem. Commun*., 2017, **53**, 1309.

4. M. W. Chorab, R. Banasz, M. Kubicki and V. Patroniak, *Electrochim. Acta*., 2017, **258**, 571.

5. K. R. Adam, *J. Phys. Chem. A*, 2002, **106**, 11963.

6. T. M. Krygowski, H. Szatylowicz and J. E. Zachara, *J. Org. Chem.*, 2005, **70**, 8859.

7. X. Ma, R. Sun, J. Cheng, J. Liu, F. Gou, H. Xiang and X. Zhou, *J. Chem. Educ*., 2016, **93**, 2, 345.

8. M. F. Khan, M. K. Singh and S. Sen, *J. Phys. Chem. B*, 2016, **120**, 1008.

9. A. Rawat and S. Maiti, *Proc. Natl. Acad. Sci., India, Sect. A Phys. Sci*., 2015, **85**, 519.

10. C. Dong and J. Irudayaraj, *J. Phys. Chem. B*, 2012, **116**, 12125.

11. S. Nandi, P. Mondal, R. Chowdhury, A. Saha, S. Ghosh and K. Bhattacharyya, *Phys. Chem. Chem. Phys*., 2016, **18**, 30444.

12. R. Vasanthi, S. Ravichandran and B. Bagchi, *J. Chem. Phys.*, 2001, **114**, 7989.

13. S. Sharma, N. Pal, P. K. Chowdhury, S. Sen and A. K. Ganguli, *J. Am. Chem. Soc.*, 2012, **134**, 19677.

14. C. Reichardt, *Chem. Rev*., 1994, **94**, 2319.

15. J. A. Olzmann and P. Carvalho, *Nat. Rev. Mol. Cell Biol.*, 2019, **20**, 137.

16. M. Collot, S. Bou, T. K. Fam, L. Richert, Y. Mély, L. Danglot and A. S. Klymchenko, *Anal. Chem.*, 2019, **91**, 1928.

17. S. Nandi, S. Ghosh and K. Bhattacharyya, *J. Phys. Chem. B*, 2018, **122**, 3023.

18. B. Das, M. N. Roy and D. K. Hazra, *Indian J. Chem. Tech*., 1994, **1**, 93.

19. B. I. Ionin, B. A. Ershov and A. I. Kol'tsov, *NMR Spectroscopy in Organic Chemistry*, Springer, 1983.